

See discussions, stats, and author profiles for this publication at: <https://www.researchgate.net/publication/40445058>

Optical Properties of the High-Pressure Phases of SnO₂: First-Principles Calculation

ARTICLE *in* THE JOURNAL OF PHYSICAL CHEMISTRY A · DECEMBER 2009

Impact Factor: 2.69 · DOI: 10.1021/jp909021r · Source: PubMed

CITATIONS

17

READS

61

8 AUTHORS, INCLUDING:



Yanlu Li

Universität Paderborn

29 PUBLICATIONS 241 CITATIONS

[SEE PROFILE](#)



Weiliu Fan

Shandong University

79 PUBLICATIONS 1,420 CITATIONS

[SEE PROFILE](#)



Pan Li

Hebei Normal University

24 PUBLICATIONS 294 CITATIONS

[SEE PROFILE](#)



Xian Zhao

Shandong University

238 PUBLICATIONS 2,011 CITATIONS

[SEE PROFILE](#)

Optical Properties of the High-Pressure Phases of SnO₂: First-Principles Calculation

Yanlu Li,[†] Weiliu Fan,^{*,‡} Honggang Sun,[†] Xiufeng Cheng,[†] Pan Li,[†] Xian Zhao,^{*,†}
Jingcheng Hao,[‡] and Minhua Jiang[†]

State Key Laboratory of Crystal Materials, Shandong University, Jinan 250100, China, and Key Laboratory of Colloid and Interface Chemistry, Ministry of Education, School of Chemistry and Chemical Engineering, Shandong University, Jinan, 250100, China

Received: September 18, 2009; Revised Manuscript Received: November 8, 2009

We present a detailed investigation on the optical properties, including dielectric function, reflectivity, absorption, refractive index, and electron energy-loss spectrum, of the high-pressure phase SnO₂ in the rutile, pyrite, fluorite, and cotunnite structures by using the density functional theory (DFT) plane-wave pseudopotential method. The results indicate that with the increasing of pressure the band gaps become larger, the density of states are broader, so the curves of optical properties have a little blue shift. Except that the fluorite phase has some metallic properties, the other three phases exhibit excellent dielectric behavior. Interestingly, the fluorite and cotunnite SnO₂ phases always have some special characteristics, such as higher plasma frequency, which need further fundamental and application research.

1. Introduction

Recently, high-pressure science has undergone a renaissance, with rapid advances in techniques and instrumentation permitting a substantial growth in the range of experiments available to high-pressure research.¹ High-pressure research is now leading to the identification of new types of physical behavior and new families of potential technological materials, often with previously unknown chemical and physical properties, having an enormous impact on many fields, such as physics, molecular chemistry, geophysics, and biology.^{2–4} Strategies will now need to be identified to probe and develop their properties in high-pressure conditions for technological applications.

Tin oxide (SnO₂), as a very attractive degenerate *n*-type semiconductor material with wide band gap (3.6 eV), has attracted increasing interests owing to its outstanding electrical, optical, and electrochemical properties and is attractive for potential applications such as catalytic support material, transparent electrodes for flat panel displays, solar cells, gas sensors, varistors and optoelectronic devices.^{5–8} Under ambient temperature and pressure, SnO₂ crystallizes in the tetragonal rutile-type structure, belonging to the *P4₂/mnm* space group, and the high-pressure behaviors of bulk SnO₂ have seen sustained investigation both in experiments and in theories, since Jiang et al.⁹ found that the tetragonal rutile-type structure could transform into the cubic pyrite phase with the space group *Pa*₃ at a pressure of 18 GPa. Moreover, Haines and Léger,¹⁰ by means of angle-dispersive X-ray diffraction analysis, demonstrated the existence of three phase transitions on compression. Rutile-type SnO₂ underwent a second-order transition to an orthorhombic CaCl₂-type (*Pnnm*) phase at 11.8 GPa under hydrostatic conditions and to an orthorhombic α -PbO₂-type (*Pbcn*) phase above 12 GPa under nonhydrostatic conditions. Both the α -PbO₂-type and the CaCl₂-type phases transformed to a modified fluorite-type phase (*Fm3m*) above 21 GPa at

ambient temperature. A recent calculation¹¹ predicted that the transition pressure from rutile to pyrite phase and to fluorite phase are under 17 and 24 GPa, respectively, and found a new transformation from the most stable phase to cotunnite-type (*Pnam*) phase under a pressure of 33 GPa.

Up until now, most of the works are devoted to the phase transition, electronic properties, elastic behaviors, lattice dynamics properties, and phonon properties.^{5–11} As an excellent optoelectronic material, it is an important aspect to refer to its optical properties. Though some experimental results of optical properties of SnO₂ have been reported^{12–17} and, recently, Roman et al.¹² studied optical properties of SnO₂ (absorption coefficient and dielectric tensor only) employing a first-principles and full-potential linearized augmented plane wave (FPLAPW) method within the local density approximation (LDA), the optical properties of high-pressure phase SnO₂ have been only barely touched. The great interest in high-pressure behavior comes from the possible repercussions for solid-state physics, crystal chemistry, and materials science. Fortunately, the first-principles method is a proper way to find some new properties under high pressures different from atmospheric pressure. Besides, it is significantly necessary for fundamental physics and potential applications to study the electronic and optical properties of high-pressure SnO₂ phases. In addition, most of the studies have focused on the properties of rutile-type, CaCl₂-type, and α -PbO₂-type phases, and more studies on optical properties of the pyrite-type, fluorite-type, and cotunnite-type SnO₂ are still required.

In this work, we calculate the structural, electronic, and optical properties of the rutile-type, pyrite-type, fluorite-type, and cotunnite-type SnO₂ phases under the respective structural phase transition pressures. The structural data, charge transfer, bond length, and bond population for ionicity are presented, since the ionicity is an important factor to determine the structural phase transition pressure. The electronic properties have also been studied with respect to the energy bands determining both the interband and intraband transitions, which influence the optical properties of phases. Then, we calculate the direct band gap of all four phases from 0 to 30 GPa to get the pressure dependence of the band gap and the hydrostatic band gap

* To whom all correspondence should be addressed. Tel: 86-531-88366330. Fax: 86-531-88364864. E-mail: X.Z., zhaoxian@icm.sdu.edu.cn; W.F., fwl@sdu.edu.cn.

[†] State Key Laboratory of Crystal Materials.

[‡] Key Laboratory of Colloid and Interface Chemistry.

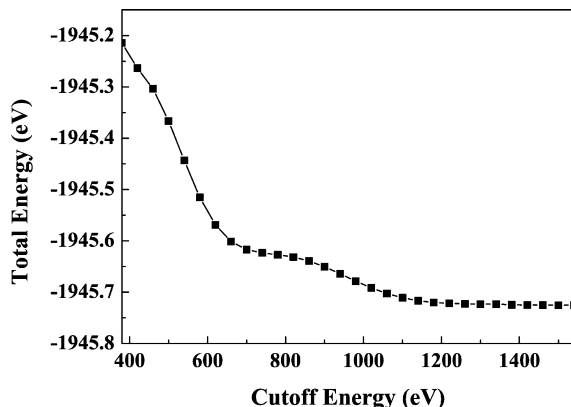


Figure 1. Convergences of the total energy of rutile phase versus the cutoff energy for the k -point mesh of $5 \times 5 \times 8$.

deformation potential. Lastly, optical properties such as the dielectric function, reflectivity, absorption, refractive index, and electron energy loss function are investigated and are compared with those of different pressures and different phases.

2. Computational Details

The first-principles density functional theory (DFT) calculations¹⁸ were employed with the Cambridge Sequential Total Energy Package (CASTEP) code,¹⁹ using Vanderbilt-type ultrasoft pseudopotentials²⁰ and a plane-wave expansion of the wave functions. We used the local-density approximation (LDA) with the Ceperley–Alder²¹ form to describe the exchange and correlation potential. The Monkhorst–Pack scheme k -point sampling was used for integration over the first Brillouin zone.²² The Kohn–Sham energy function was directly minimized via the conjugate-gradient method.¹⁹ The convergence criteria for structure optimization and energy calculation were set to ultrafine quality with the k -point mesh of $5 \times 5 \times 8$ for the rutile structure, $6 \times 6 \times 6$ for the pyrite structure, $6 \times 6 \times 6$ for the fluorite structure, and $3 \times 3 \times 6$ for the cotunnite structure, which make the tolerance for self-consistent field, energy, maximum force, maximum displacement, and maximum stress to be 5.0×10^{-7} eV/atom, 5.0×10^{-6} eV/atom, 0.01 eV/Å, 5.0×10^{-4} Å, and 0.02 GPa, respectively. It was found that the cutoff energy had a serious effect on the convergence of our calculations, so we investigated the dependences of the total energy on the cutoff energy. As an example, the results are plotted in Figure 1, for the rutile SnO₂. It can be seen that with the k -point set mesh fixed at $5 \times 5 \times 8$, the change in total energy is less than 2 meV when the cutoff energy is higher than 1300 eV. In consideration of computational cost, we choose the cutoff energy to be in 1300 eV.

3. Results and Discussion

3.1. Structural Properties and Population Analyses. The structures of the rutile, pyrite, fluorite, and cotunnite SnO₂ phases under the respective phase transition pressures are shown in Figure 2. At ambient pressure, SnO₂ crystallizes in the rutile structure, which has a tetragonal symmetry, with the $P4_2/mnm$ space group, as shown in Figure 2a. In this phase, the Sn site is surrounded by six O atoms, with four in a plane (Sn–O: 2.023 Å, shown in Table 1) and two along an axis perpendicular to that plane (Sn–O: 2.030 Å). SnO₂ undergoes a structural phase transition to pyrite-type phase (Figure 2b) at 17 GPa, with space group $Pa\bar{3}$ and exhibits a reconstructive character. Different from the rutile phase, the Sn site is surrounded by six equidistant O atoms with the bond length Sn–O 2.044 Å. Figure

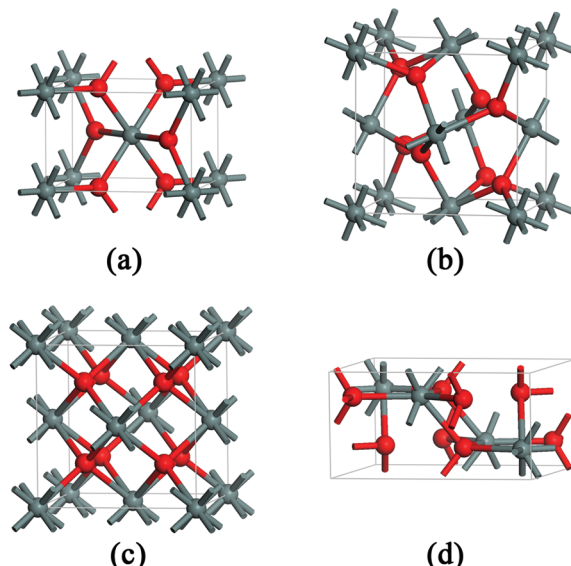


Figure 2. Bulk structures of the SnO₂ polymorphs (gray and red colors represent Sn and O atoms, respectively): (a) rutile-type ($P4_2/mnm$) under 0 GPa; (b) pyrite-type ($Pa\bar{3}$) under 17 GPa; (c) fluorite-type ($Fm\bar{3}m$) under 24 GPa; (d) cotunnite-type ($Pnam$) under 33 GPa.

2c gives the fluorite-type structure with the space group $Fm\bar{3}m$ in which Sn⁴⁺ is centered in a perfect cubic symmetry, and the distance of Sn–O is 2.153 Å. Figure 2d indicates the orthorhombic cotunnite-type structure at 33 GPa with the space group $Pnam$. In this phase, nine oxygen anions place around the Sn⁴⁺ cation, and form six types of Sn–O bonds (as shown in Table 1).

The structures are optimized under the structural phase transition pressures of 17 GPa for the pyrite structure, 24 GPa for the fluorite structure, and 33 GPa for the cotunnite structure. The calculated lattice constants, charge transfer, bond lengths and bond population of the rutile, pyrite, fluorite and cotunnite SnO₂ phases under different pressures near the structural transition are shown in Table 1. These values agree well with experimental value and other calculation value, indicating that the methods used in our calculations are reliable and reasonable.

It is well-known that, under ambient pressure, the highly covalent materials favor the lower coordination structures, whereas the highly ionic materials have a tendency to favor the higher coordination structures. Covalent materials could be transformed into the higher coordination phases via the high pressure method. Therefore, the structural phase transition pressure should be determined by the degree of ionicity being an important factor. So, we investigated the charge and chemical bonding of the rutile, pyrite, fluorite, and cotunnite SnO₂ phases using the Mulliken population analysis in detail. We confess that the absolute magnitudes of the atomic charges yield by the population analysis have little physical meaning, but we can find some useful information from the relative values of Mulliken population.

From Table 1, it can be seen that with the increase of the external pressure the lattice constants become small and the charge transfer is increased. When the rutile phase is compressed under pressure from 0 to 33 GPa, the charge transfer from Sn to O increases from 0.93 to 0.96 and the Sn–O bond length is compressed from 2.023 to 1.939 Å and from 2.030 to 1.974 Å, respectively. It is interesting that the bond population is up from 0.34 to 0.37 for the first type Sn–O bond, whereas it is 0.75 all the time for the second type when the pressure is from 0 to 33 GPa, implying that pressure has little effect on the ionicity of

TABLE 1: Structural Data of the Rutile, Pyrite, Fluorite, and Cottunite SnO_2 Phases at Ambient Pressure and the Phase Transition Pressures^a

	rutile $P4_3/mnm$						pyrite $P\bar{a}\bar{3}$						fluorite $Fm\bar{3}m$						cottunite $Pnam$							
	0 GPa			0 GPa			0 GPa			0 GPa			0 GPa			0 GPa			0 GPa			0 GPa				
	expt	calc	17 GPa calc	24 GPa calc	33 GPa calc	expt	calc ^d	17 GPa calc	expt ^c	calc ^d	24 GPa calc	expt ^c	calc ^d	24 GPa calc	expt ^c	calc ^d	24 GPa calc	expt ^c	calc ^d	24 GPa calc	expt ^c	calc ^d	24 GPa calc	expt ^c	calc ^d	
<i>a</i>	4.737 ^b	4.715 ^d	4.564	4.527	4.484	5.085 ^c	5.066	4.914	5.087	4.993	4.849	5.016	5.326	5.185												
<i>b</i>		4.689 ^b							4.972																	
<i>c</i>	3.186 ^b	3.194 ^d	3.111	3.099	3.086																					
$B_0 (B_0')$	205 (7) ^b	221 (6) ^d	245 (5)	$I_1 = 2.023$	$I_1 = 1.973$	$I_1 = 1.957$	$I_1 = 1.939$	328 (4) ^b	281 (3)	290 (10) ^c	271 (5)	2.044	2.008	2.153	2.100	2.100	2.100	2.029	$I_1 = 2.039$							
Sn–O length																										
	$I_2 = 2.030$	$I_2 = 1.998$	$I_2 = 1.987$					$I_2 = 1.974$																		
Sn–O population	$p_1 = 0.34$	$p_1 = 0.36$	$p_1 = 0.37$		$p_1 = 0.37$			$p_1 = 0.37$		$p_1 = 0.39$		$p_1 = 0.38$		$p_1 = 0.39$		$p_1 = 0.39$		$p_1 = 0.38$		$p_1 = 0.38$		$p_1 = 0.38$		$p_1 = 0.29$		
charge transfer	0.93	0.94	0.95					0.96		0.90		0.92		0.88		0.90										

^aLattice parameters *a*, *b* and *c* are in Å; zero-pressure bulk modulus values B_0 are in GPa; Sn–O bond lengths are in Å. ^bReference 10. ^cReference 9. ^dReference 11. ^eReference 11. Our results are presented in bold.

the second type of Sn–O bonds. With regard to the pyrite and the fluorite SnO₂ phases, the charge transfer and the bond population are also increased while the bond length is reduced when the pressure increases. This can be easily explained: when the bond length is shorter, more charge transfer from Sn atoms to O atoms occurs because of more electron cloud overlap. For the fluorite phase, the bond population is 0.27, smaller than the other phases, indicating more ionic nature. It is worth noting that when the cotunnite structure is compressed from 0 to 33 GPa, great changes have taken place in the type of bonding with Sn and O, though the number of the Sn–O bond type is still six. This phenomenon illuminates that the degree of electron cloud overlap and bonding between the neighboring atoms change under external pressure. This may lead to significant change in the inherent nature of materials and has far-reaching research and application value.

In addition, we have generated the values of the zero-pressure bulk modulus B_0 and its pressure derivative B'_0 , by means of a numerical fitting procedure that is consistent with the Birch–Murnaghan²³ EOS:

$$P = \frac{3}{2}B_0(r^{7/3} - r^{5/3})\left[1 + \frac{3}{4}(B'_0 - 4)(r^{2/3} - 1)\right]$$

where $r = V_0/V$.

Our theoretical results show that the rutile-type, pyrite-type, and fluorite-type phases present high bulk modulus values (derivative B'_0) of 245(5), 271(5), and 269(5) GPa, whereas other calculation values are 221(6), 281(3), and 288(6) GPa.¹¹ Our B_0 values of rutile and pyrite phases are close to the experimental values of 270 and 290 GPa from ref 9. The bulk modulus of cotunnite phase is 136(4) GPa, which is much smaller than the other three phases. Our result agrees well with the previous 180(8) GPa¹¹ but also has obvious underestimation of the experimental values 417(4) GPa.²⁴

3.2. Electronic Properties. The energy bands determine both the interband and intraband transitions, which influence the optical properties of phases. The effect of the pressure on the band structures of all polymorphs has been examined in the present study, so the effect of the pressure on the optical properties is clear. The effect of the pressure on the band structures of all polymorphs has been examined in the present study. The calculated bulk SnO₂ band structures along the symmetry lines of the rutile, pyrite, fluorite, and cotunnite phases are illustrated in Figure 3. The Fermi level is chosen to be the zero of the energy scale.

From the band structure of the rutile SnO₂ phase shown in Figure 3a, we find that the direct band gap energy (E_g) is 1.38 eV at the highly symmetric Γ -point, which is much smaller than 3.6 eV from the experimental band gap result of the rutile SnO₂ phase.²⁵ The usual problem of the DFT gap underestimation is observed. The pyrite-type and cotunnite-type SnO₂ are also direct band gap semiconductors at the respective phase transition pressure 17 and 33 GPa, and the direct band gap E_g value is 1.90 eV (Figure 3b) and 1.64 eV (Figure 3d) at the Γ -point, respectively. As shown by the band structure of the fluorite phase at 24 GPa in Figure 3c, it is an indirect band gap semiconductor, with the direct band gap 3.03 eV at Γ -point and the smallest indirect band gap is 1.32 eV. However, to the best of our knowledge, so far there are no experimental data available that could verify these calculated results.

Schweitzer et al.²⁶ have determined the pressure dependence of the band gap and the exciton binding energy for the rutile SnO₂ using two-photon spectroscopy. The hydrostatic band gap deformation potential, a_g , can be defined as the product of the

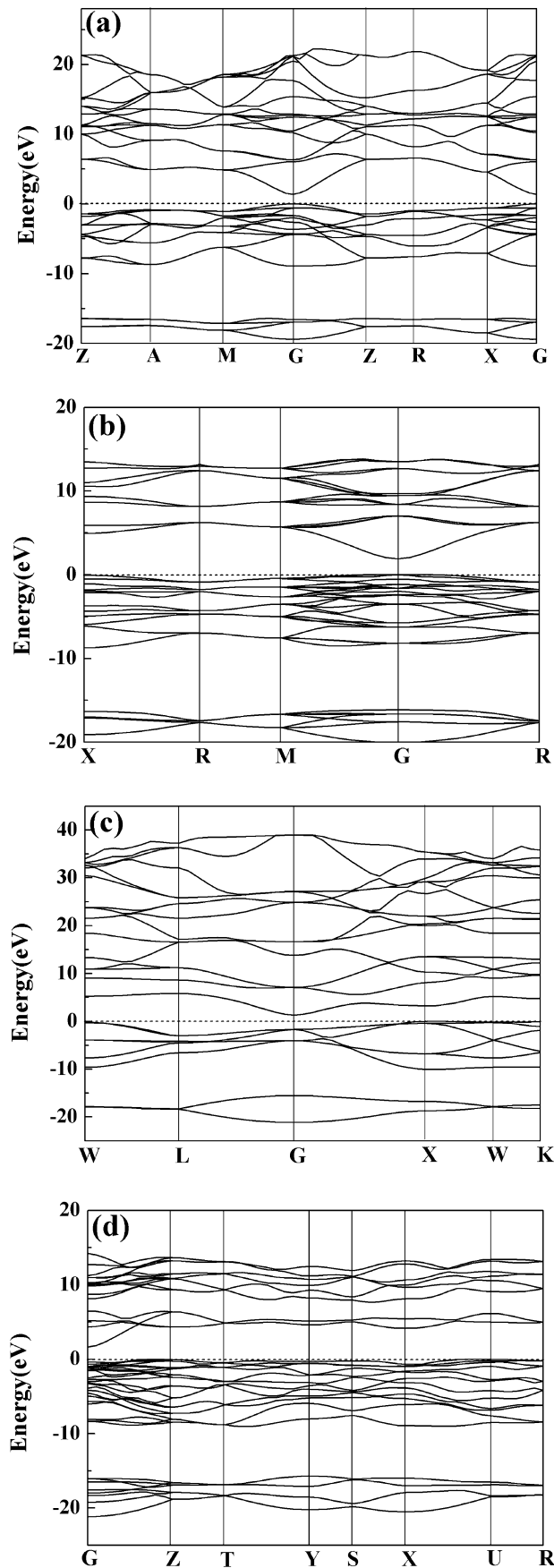


Figure 3. Band structures of the SnO₂ polymorphs: (a) rutile-type at ambient pressure; (b) pyrite-type at 17 GPa; (c) fluorite-type at 24 GPa; (d) cotunnite-type at 33 GPa.

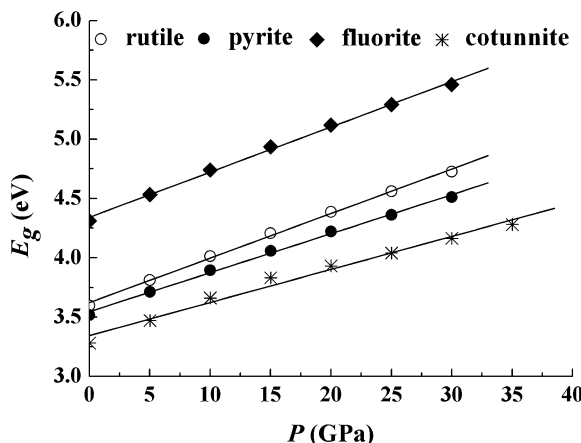


Figure 4. Effect of the pressure on the band gap energy for the SnO_2 polymorphs.

bulk modulus and the variation of the band gap, E_g , with pressure, $a_g = B_0 (dE_g/dP)$. To describe the band gap deformation potential and the optical properties accurately, a usual empirical correction is introduced, namely, the scissors operator,²⁷ which basically means to adjust the band gap with a constant potential to reproduce the experimental energy band gaps. This operator is often used in the determination of the band gap offsets.^{28,29} Compared with the experimental band gap value for the rutile-type phase at ambient pressure, we choose the scissors operator as 2.22 eV.

Figure 4 shows the effect of the pressure on the direct band gap energy for the SnO_2 polymorphs. We find an increase of the E_g value with pressure in all structures as the conduction band moves to higher energy values. For rutile SnO_2 , the linear fit gives $dE_g/dP = 0.0376 \text{ eV/GPa}$ using the scissors operator. Considering the bulk modulus of 245 GPa obtained from the above-mentioned formula, the linear pressure coefficient converts to the gap deformation potential of $B_0 (dE_g/dP) = 9.21 \text{ eV}$, which is a little smaller than the experimental data, 13.16 eV.²⁶ Such a high value is typical for III–VI semiconductors. Using the same method, we could find that the hydrostatic band gap deformation potentials are 9.39, 10.08, and 3.79 eV for pyrite-type, fluorite-type, and cotunnite-type, respectively. The results for rutile-type, pyrite-type, and fluorite-type agree well with other theoretical values of 10.12, 12.34, and 12.38 eV, while the other calculation value 7.31 eV of cotunnite-type SnO_2 ¹¹ is nearly 2 times larger than our gap deformation potential value. This difference is mainly from the different way in fitting the dE_g/dP value and the different calculated B_0 values, which are considered to be reasonable and acceptable.

The density of states (DOS) of the rutile, pyrite, fluorite, and cotunnite structures at the phase transition pressure are plotted in Figure 5. In the valence bands (VBs) of all the four phases, O 2s states are dominant below -15 eV with a slight contribution of the Sn 5s and Sn 5p states; in the range between -10 and 0 eV , the O 2p states are the most dominant, especially at the region closer to the Fermi energy level (E_F), while a hybridization between Sn 5s, Sn 5p, and O 2p states could be seen in the range of -10 eV . The density of states of the conduction bands (CBs) are mainly derived from Sn 5s and Sn 5p orbitals while O 2p states also have a little contribution. For the three high-pressure phases, obvious hybridization between Sn 5s and O 2p states can be observed in the bottom of CBs. As Figure 5a–d shows, when the rutile SnO_2 is compressed from 0 to 33 GPa, the peaks of DOS in the valence bands have a tendency to shift to the lower energy (red shift). For instance,

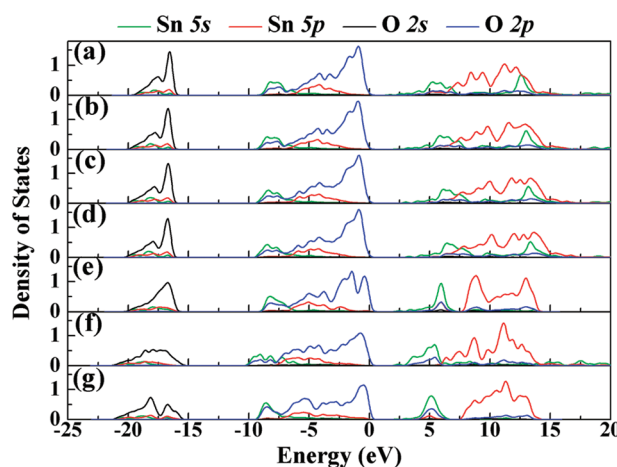


Figure 5. DOSs of O 2s, O 2p, and Sn 5s, Sn 5p: (a) rutile phase at 0 GPa; (b) rutile phase at 17 GPa; (c) rutile phase at 24 GPa; (d) rutile phase at 33 GPa; (e) pyrite phase at 17 GPa; (f) fluorite phase at 24 GPa; (g) cotunnite phase at 33 GPa.

for the O 2s orbitals, the two peaks are shifted from -16.57 to -16.73 eV and from -17.53 to -17.95 eV , respectively, and the two highest peaks of the O 2p orbitals are shifted from -0.92 to -0.87 eV and from -4.14 to -4.15 eV , respectively. In the CBs, with the increasing pressure, the peaks of the Sn 5s and Sn 5p orbitals are slightly broadened and the intensities are slightly decreased. However, the changes in the DOS peaks are a bit more complicated at the transition pressures of SnO_2 polymorphs. Under 17 GPa, the intensity of the highest peak of O 2s orbitals for the pyrite phase is lower than that for the rutile phase, and the pyrite phase's secondary highest peak of O 2s orbitals has disappeared. For the pyrite phase, two high peaks of O 2p orbitals could be observed and their intensities are all lower than that of the highest peak of rutile phase's O 2p orbitals. Sn 5s orbitals are dominant at the bottom of the CBs and two sharp peaks of Sn 5p orbitals appear, whereas there are a series of peaks of Sn 5p orbitals in the rutile structure. Besides, the peaks of the Sn 5s and Sn 5p orbitals are obviously enhanced and become narrow for pyrite SnO_2 . For the fluorite structure under 24 GPa, the height of peaks of O 2s and O 2p orbitals in the VBs become small, and the peaks of Sn 5s and Sn 5p orbitals enhanced. Moreover, with obvious broadening of the whole DOS, two peaks of Sn 5p orbitals are obviously observed at 11.11 and 8.71 eV , and the peak of Sn 5s orbitals at 13.18 eV has disappeared. The changes of DOS for the cotunnite structure under 33 GPa are similar to that for the fluorite structure under 24 GPa. Differently, the DOS in the CBs becomes narrow, and the position of the highest and secondary highest peaks of O 2s orbitals in the VBs have been exchanged.

To investigate the electronic states in detail, we calculated the electron density difference for SnO_2 polymorphs in Figure 6. The planes containing more Sn–O bonds are chosen to construct the contour plots. From Figure 6a we can see that for rutile-type SnO_2 , with increasing pressure the charge transfer from Sn to O also increases and there are more degrees of covalent bonding between Sn and O. The same phenomenon could be observed for pyrite-type and fluorite-type SnO_2 , so this picture confirms our analysis in bond population. Interestingly, a different case occurs for the cotunnite structure. Figure 6d displays a distinct reduction of the degree of covalent bonding of Sn–O, and we notice that some population values of Sn–O bonds become smaller when the pressure increases (from Table 1), so we can properly explain why cotunnite structure

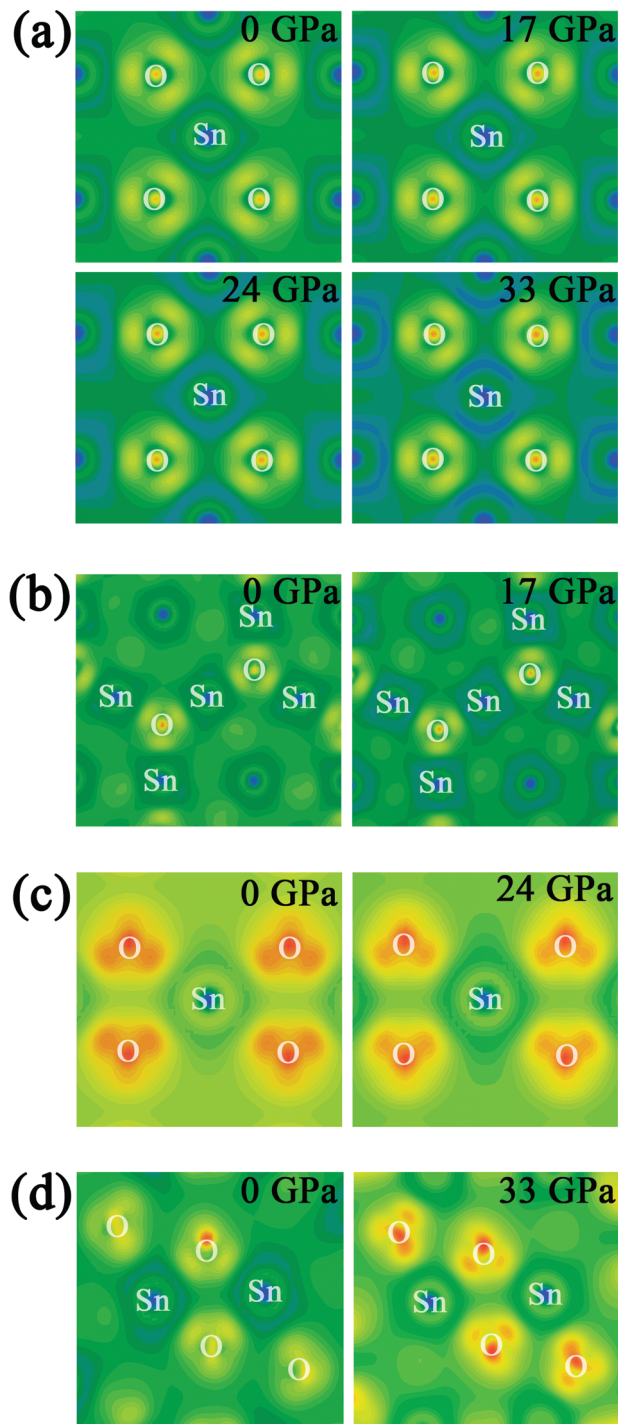


Figure 6. Electron density difference contour maps from -3.578×10^{-1} (blue) to 4.717×10^{-1} (red) e Å⁻³ for SnO₂ polymorphs: (a) rutile-type; (b) pyrite-type; (c) fluorite-type; (d) cotunnite-type.

demonstrates an opposite nature in electron density difference. Meanwhile, stronger ionic nature, which may be caused by the longer Sn–O bond length for fluorite phase, could also be found in Figure 6c.

3.3. Optical Properties. Pressure-dependent structural phase transition may lead to different selection rules, which together with the altered density and band hybridization may bring some special optical properties and potential application.³⁰ That is why we discuss the optical properties of high-pressure SnO₂ in detail. We could describe the interaction of a photon with the electrons in terms of time-dependent perturbations of the ground-state electronic states. The electric field of the photon leads to the

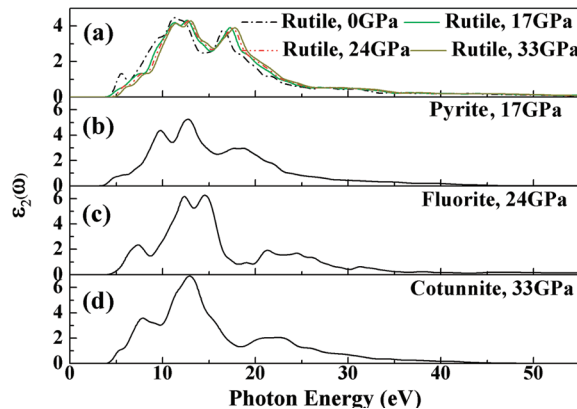


Figure 7. Imaginary part of dielectric function $\varepsilon_2(\omega)$: (a) rutile structure from 0 to 33 GPa; (b) pyrite structure under 17 GPa; (c) fluorite structure under 24 GPa; (d) cotunnite structure under 33 GPa.

transition between occupied and unoccupied states, including plasmons and single particle excitations. The excitation spectra can be described as a joint DOS between the valence and conduction bands. We could obtain the imaginary part $\varepsilon_2(\omega)$ of the dielectric function from the momentum matrix elements between the occupied and unoccupied wave functions, and the real part $\varepsilon_1(\omega)$ of the dielectric function can be evaluated from $\varepsilon_2(\omega)$ using the Kramer–Kronig relations.³¹ Arising from $\varepsilon_1(\omega)$ and $\varepsilon_2(\omega)$, all the other optical properties, such as reflectivity $R(\omega)$, absorption coefficient $\alpha(\omega)$, the real part of the refractive index $n(\omega)$, the imaginary part of the refractive index $k(\omega)$, and energy-loss spectrum $L(\omega)$, can be calculated.^{32,33}

$$\begin{aligned} R(\omega) &= \left| \frac{\sqrt{\varepsilon_1(\omega) + j\varepsilon_2(\omega)} - 1}{\sqrt{\varepsilon_1(\omega) + j\varepsilon_2(\omega)} + 1} \right|^2 \\ \alpha(\omega) &= \sqrt{2}\omega[\sqrt{\varepsilon_1^2(\omega) + \varepsilon_2^2(\omega)} - \varepsilon_1(\omega)]^{1/2} \\ n(\omega) &= [\sqrt{\varepsilon_1^2(\omega) + \varepsilon_2^2(\omega)} + \varepsilon_1(\omega)]^{1/2}/\sqrt{2} \\ L(\omega) &= \varepsilon_2(\omega)/[\varepsilon_1^2(\omega) + \varepsilon_2^2(\omega)] \end{aligned}$$

The imaginary part of dielectric function $\varepsilon_2(\omega)$ is the basic of the optical properties for any materials. Figure 7 shows the imaginary part of the complex dielectric function of the SnO₂ polymorphs directly obtained from the electronic structure calculations. From Figure 7a, we can find that at ambient pressure, there are two peaks at 11.26 and 16.69 eV for the rutile phase. The peak at 11.26 eV mainly arises from the electron transition from the O 2p orbitals to Sn 5p orbitals, and the electron transition from the hybridization orbitals of O 2p and Sn 5p to the hybridization orbitals of Sn 5s and Sn 5p may lead to the peak at 16.69 eV. When it is compressed from 0 to 33 GPa, the line shape of $\varepsilon_2(\omega)$ is almost the same while there is a little shift toward the high-energy region (blue shift). The plot of the pyrite structure at 17 GPa shows three main peaks at around 9.75, 12.73, and 18.69 eV, respectively, as shown in Figure 7b. Combined with the analysis of DOS, we can get that the electron transition from O 2p to Sn 5p orbitals leads to the peak at 9.75 and 12.73 eV, while the electron transition from the hybridization orbitals of O 2p and Sn 5p to Sn 5p orbitals leads to the peak at 18.69 eV. For the fluorite SnO₂ at 24 GPa, there are two remarkable high peaks at about 12.32 and 14.56 eV, which indicates that the fluorite structure under 24 GPa may have some interesting characteristics. The shape of the plot for the cotunnite phase under 33 GPa is similar to

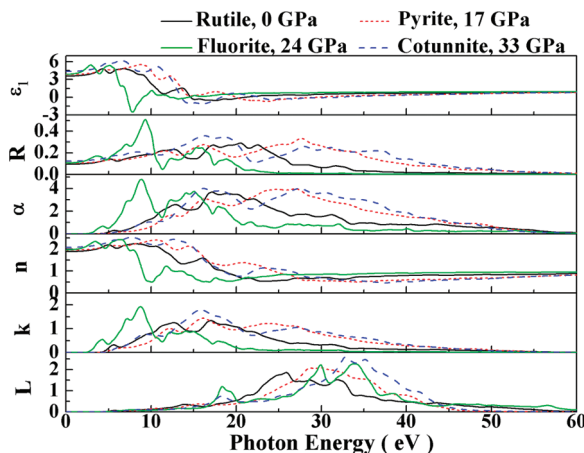


Figure 8. Real part of the dielectric function $\epsilon_1(\omega)$, reflectivity $R(\omega)$, absorption coefficient $\alpha(\omega)$, real part of the refractive index $n(\omega)$, imaginary part of the refractive index $k(\omega)$, and electron energy-loss functions $L(\omega)$ of the rutile phase at 0 GPa, pyrite phase at 17 GPa, fluorite phase at 24 GPa, and cotunnite phase at 33 GPa.

that for the pyrite phase under 17 GPa, reminding us that they may have some analogous optical properties in the specific aspect.

The real part of the dielectric function $\epsilon_1(\omega)$, reflectivity $R(\omega)$, absorption coefficient $\alpha(\omega)$, the real part of the refractive index $n(\omega)$, the imaginary part of the refractive index $k(\omega)$, and energy-loss spectrum $L(\omega)$ of the rutile phase at 0 GPa, pyrite phase at 17 GPa, fluorite phase at 24 GPa, and cotunnite phase at 33 GPa are plotted in Figure 8. The $\epsilon_1(\omega)$ of the rutile phase of SnO_2 , which is quite similar to those of the pyrite and cotunnite structures, has a series of small peaks from 0 to 15 GPa and exhibits excellent dielectric behavior. However, from the $\epsilon_1(\omega)$ of the fluorite structure at 24 GPa, we can find a sharp peak below zero at about 15.90 eV, at which the material has metallic properties. The reflectivity spectrum of the fluorite SnO_2 under 24 GPa is narrower than that for the rutile phase at ambient pressure; the former is about 0–25 eV while the latter is about 0–45 eV. In contrast, the pyrite and cotunnite phases have broader reflective ranges from 0 to 60 eV. The span of reflectivity for SnO_2 has some responding relationship with the energy band gap, namely, the smaller the band gap is, the narrower the energy scale of reflectivity is. Moreover, there are two main peaks of the fluorite SnO_2 at 16.41 and 27.06 eV, which could be interpreted as the electron transitions from the valence to conduction bands and the interband transitions, respectively. All four SnO_2 phases have absorption bands up to 60 eV, indicating that it is difficult to observe transparent SnO_2 crystal under experimental pressure. The absorption spectrum of the fluorite SnO_2 contains two main peaks at around 15.58 and 26.55 eV, and their intensities are stronger than those of the highest peaks of the other three phases. In the dispersion curve of the refractive index, the fluorite structure still exhibits features different from the others.

Besides, the electron energy-loss function $L(\omega)$ is also an important optical parameter describing the energy loss of a fast electron traversing a certain material, and the peaks in $L(\omega)$ spectra represent the characteristics associated with the plasma resonance. In addition, the positions of peaks in $L(\omega)$ spectra, which correspond to the so-called plasma frequency, point out the transition from the metallic property [$\epsilon_1(\omega) < 0$] to the dielectric property [$\epsilon_1(\omega) > 0$] for a material. Moreover, the peaks of $L(\omega)$ correspond to the trailing edges in the reflection spectra; for instance, the peaks of $L(\omega)$ for the rutile structure

are at 25.88 and 31.89 eV, corresponding to the abrupt reduction of $R(\omega)$ and the steady value of reflectivity, respectively. For the fluorite phase, three main peaks at 18.39, 29.93, and 33.89 eV also indicate the reduction from starting to ending of reflectivity. With regard to the pyrite and cotunnite structure, broad peaks correspond to the slow descent of reflectivity.

4. Conclusion

On the basis of quantum chemical simulations, we provide the systematic investigation of the structural, electronic, and optical properties of the rutile, pyrite, fluorite, and cotunnite SnO_2 phases at their structural phase transition pressures by the first-principles method. The dielectric function and optical properties such as reflectivity, absorption coefficient, refractive index, and electron energy-loss function are presented in a wide energy range. Our results reveal that the curves of optical properties have a tendency to blue shift with increasing external pressure. Except that the fluorite phase has some metallic properties, the other three phases exhibit excellent dielectric behavior. We also find some relationship between the energy band gap and reflectivity; namely, the smaller band gap, the narrower the energy scale of reflectivity. The absorption data indicate that it is difficult to observe transparent SnO_2 crystal under experimental pressure. Calculating the electronic and optical properties, we presume that the rutile and pyrite phases have similar features, while the fluorite and cotunnite SnO_2 phases have other special traits, such as higher plasma frequency.

Acknowledgment. This work is supported by the National Natural Science Foundation of China (Grant Nos. 50802056 and 50721002), 973 Program of China under Grant No. 2009CB930103, Natural Science Foundation of Shandong Province of China under Grant No. Y2007B08, and the Specialized Research Fund for the Doctoral Program of Higher Education of China under Grant No. 20070422060.

References and Notes

- (1) McMillan, P. F. *Nat. Mater.* **2002**, *1*, 19.
- (2) Hemley, R. J.; Ashcroft, N. W. *Phys. Today* **1998**, *51*, 26.
- (3) Isaak, Donald G. *Ultrahigh-Pressure Mineralogy: Physics and Chemistry of the Earth's Deep Interior*; Mineralogical Society of America: Washington DC, 1998.
- (4) Hemley, R. J. *Annu. Rev. Phys. Chem.* **2000**, *51*, 763.
- (5) Jarzebski, Z. M.; Marton, J. P. *J. Electrochem. Soc.* **1976**, *123*, 199C, 299C, 333C.
- (6) Hamberg; Gramquist, C. G. *J. Appl. Phys.* **1986**, *60*, R123.
- (7) Madou, M. J.; Morison, S. Y. *Chemical Sensing with Solid State Devices*; Academic Press: San Diego, 1989.
- (8) Bataille, M.; Diebold, U. *Prog. Surf. Sci.* **2005**, *79*, 47.
- (9) Jiang, J. Z.; Gerward, L.; Olsen, J. S. *Scr. Mater.* **2001**, *44*, 1983.
- (10) Haines, J.; Léger, J. M. *Phys. Rev. B* **1997**, *55*, 11144.
- (11) Gracia, L.; Beltrán, A.; Andrés, J. *J. Phys. Chem. B* **2007**, *111*, 6479.
- (12) Roman, L. S.; Valaski, R.; Canestraro, C. D.; Magalhães, E. C. S.; Persson, C.; Ahuja, R.; da Silva, E. F., Jr.; Pepe, I.; Ferreira da Silva, A. *Appl. Surf. Sci.* **2006**, *252*, 5361.
- (13) Zhitomirsky, V. N.; Çetinörgü, E.; Boxman, R. L.; Goldsmith, S. *Thin Solid Films* **2008**, *516*, 5079.
- (14) Rani, S. J.; Puri, N. K.; Somnath, C. R.; Bhatnagar, M. C.; Kanjilal, D. *Nucl. Instrum. Methods Phys. Res. B* **2008**, *266*, 1987.
- (15) Li, Y.; Zhao, Y. H.; Zhang, Z. H.; Liu, W.; Ortalan, V.; Zhou, Y. Z.; Ma, X. L.; Lavernia, E. J. *J. Cryst. Growth*. **2008**, *310*, 4226.
- (16) Feng, X. J.; Ma, J.; Yang, F.; Ji, F.; Luan, C.; Ma, H. *J. Cryst. Growth*. **2008**, *310*, 295.
- (17) Yadav, J. B.; Patil, R. B.; Puri, R. K.; Puri, V. *Mater. Sci. Eng., B* **2007**, *139*, 69.
- (18) Payne, M. C.; Teter, M. P.; Allan, D. C.; Arias, T. A.; Joannopoulos, J. D. *Rev. Mod. Phys.* **1992**, *64*, 1045.
- (19) Segall, M.; Lindan, P.; Probert, M.; Pickard, C.; Hasnip, P.; Clark, S.; Payne, M. *J. Phys.: Condens. Matter.* **2002**, *14*, 271.
- (20) Vanderbilt, D. *Phys. Rev. B* **1990**, *41*, 7892.
- (21) Ceperley, D. M.; Alder, B. J. *Phys. Rev. Lett.* **1980**, *45*, 566.

- (22) Monkhorst, H. J.; Pack, J. *Phys. Rev. B* **1976**, *13*, 5188.
(23) Birch, F. *J. Geophys. Res.* **1952**, *57*, 227.
(24) Shieh, S. R.; Kubo, A.; Duffy, T. S.; Prakapenka, V. B.; Shen, G. *Phys. Rev. B* **2006**, *73*, 014105.
(25) Agekyan, V. T. *Phys. Status Solidi A* **1977**, *43*, 11.
(26) Schweitzer, C.; Reimann, K.; Steube, M. *Solid State Commun.* **1999**, *110*, 697.
(27) Lanoo, M.; Schllüter, M.; Sham, L. J. *Phys. Rev. B* **1985**, *32*, 3890.
(28) Wei, S. H.; Zunger, A. *Phys. Rev. B* **1997**, *55*, 13605.
(29) Albanesi, E. A.; Lambrecht, W. L.; Segall, B. *J. Vac. Sci. Technol. B* **1994**, *12*, 2470.
(30) Jaffe, J. E.; Pandey, R.; Kunz, A. B. *Phys. Rev. B* **1991**, *43*, 14030.
(31) Yu, P. Y.; Cardona, M. *Fundamentals of Semiconductors*; Springer-Verlag: Berlin, 1996.
(32) Saha, S.; Sinha, T. P. *Phys. Rev. B* **2000**, *62*, 8828.
(33) Cai, M. Q.; Yin, Z.; Zhang, M. S. *Appl. Phys. Lett.* **2003**, *83*, 2805.

JP909021R